GPS Research and Monitoring of the Yellowstone Volcanic System, WY-ID-MT, and the Wasatch Fault, UT

A White Paper

Christine M. Puskas, Robert B. Smith, Wu-Lung Chang, and Jamie Farrell
University of Utah Seismology and Active Tectonics Research Group
University of Utah
Salt Lake City, Utah

October 14, 2010

Introduction

The University of Utah operates two Global Positioning System (GPS) networks of permanent stations: one in the Yellowstone volcanic field, Yellowstone National Park, Wyoming, Montana, and Idaho, and the second spanning the Wasatch fault (Wasatch Front) of northern and central Utah. The Yellowstone volcanic field and the Wasatch fault and are actively deforming regions of the Basin-Range extensional tectonic regime with high seismic hazards and a superimposed volcanic hazard at Yellowstone. These GPS networks are supplemented by temporary GPS arrays that have been operated during field campaigns since 1987.

The University of Utah GPS networks are the key elements of crustal deformation monitoring of the Yellowstone hotspot and Wasatch fault zone, designed to measure ground deformation in parallel with seismic monitoring networks operated by the University of Utah Seismograph Stations (UUSS). Ground deformation is related to active volcanic processes and faulting in Yellowstone, and to faulting in Utah, hence the importance of GPS measurements in understanding the distribution of volcanic and hydrothermal features, active faults, contemporary fault loading, fault geometry, etc. The Yellowstone and Wasatch networks extend across seismically active regions, with the potential for moderate to large earthquakes as documented in historic and Late Quaternary geologic time. Moreover, magmatic and hydrothermal activity at Yellowstone produces up to centimeters per year of deformation. Thus GPS data provide important constraints on modeling and interpretation of active Yellowstone volcanic processes.

This report provides an overview of the University of Utah GPS monitoring of these active geologic regions, including network operations, data recording and processing, a summary of data products, and a synopsis of key research findings based on our GPS measurements.

Earthquakes and Volcanism in Yellowstone and the Wasatch Fault

Earthquakes in the Yellowstone and the Wasatch fault regions are part of the Intermountain Seismic Belt (ISB), a 1400-km long geographic region of earthquakes and active faulting extending from southern Utah north to Montana that bounds the actively extending Basin-Range Province to the west and stable North America to the east [*Smith and Arabasz*, 1991]. The ISB is thus a region of elevated seismic hazard and active crustal deformation.

The Yellowstone-Snake River Plain (YSRP) volcanic field is a 17 Ma track of explosive silicic volcanic centers that formed as the North America plate moved southwest across the Yellowstone mantle hotspot (Figure 1) [*Smith and Braile*, 1994; *Smith et al.*, 2009]. The current center of YSRP volcanic activity is centered at the Yellowstone Plateau in Yellowstone National Park [*Christiansen*, 2001, 2007].

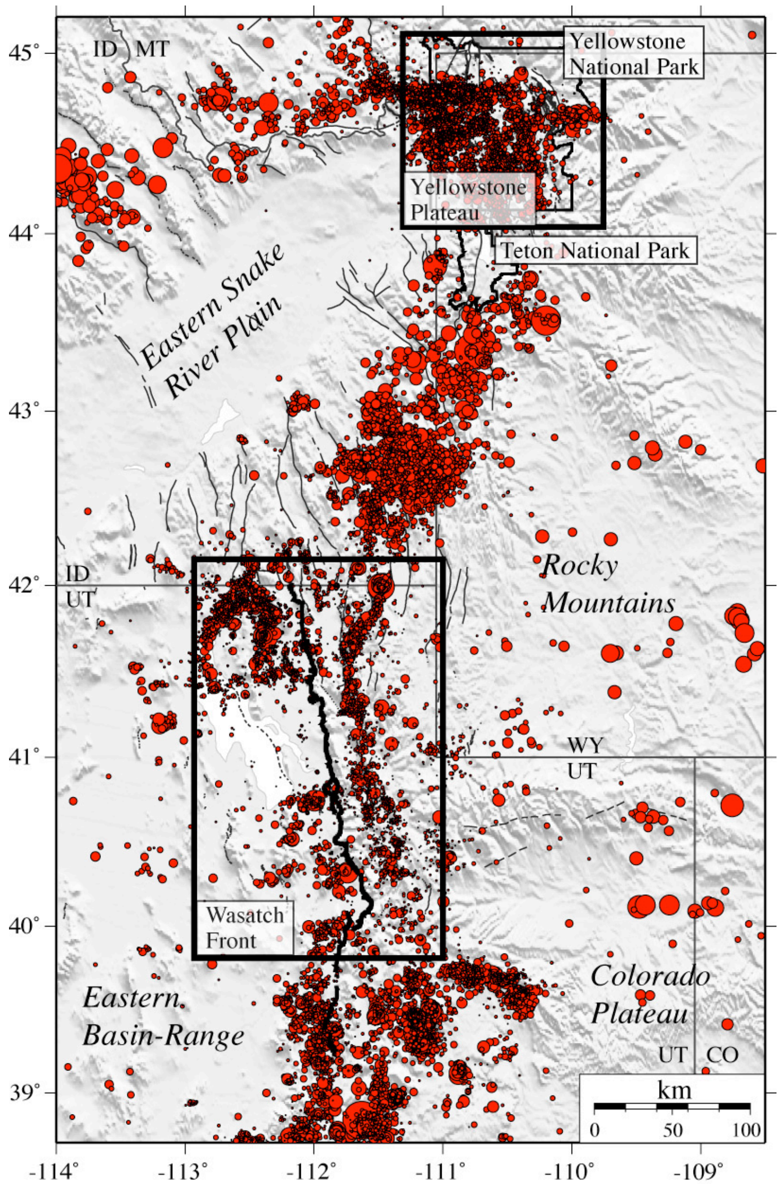

Figure 1. Index map showing topography, earthquakes, and faults in the Intermountain seismic belt. The Yellowstone Plateau and Wasatch Front are marked by boxes. The Wasatch fault is represented by the heavy line in Utah. Earthquakes (81,411 events from the UUSS catalog, 1981-2010) of the Intermountain seismic belt are represented by red circles. Tectonic provinces are labeled in italics.

Yellowstone National Park is subject to a variety of geologic hazards because of its combination of tectonic and volcanic activity: large earthquakes, hydrothermal explosions, and volcanic eruptions ranging in style from small lava flows of a few cubic kilometers to giant, caldera-forming explosive eruptions of over 1000 cubic kilometers. Over 3 million people visit Yellowstone annually, primarily in the summer. Because Yellowstone National Park is remote and the majority of the population is transient, there is limited infrastructure to deal with large-scale disasters. Thus an understanding of its geologic hazards is critical for emergency preparedness.

The Wasatch Front, centered on the Late Cenozoic Wasatch fault, is an urban corridor in northern Utah (Figure 1). Approximately 2.2 million people, or 80% of the population of Utah, live along the populated Wasatch Front, including Salt Lake City. The population is concentrated in cities built upon deep alluvial basins bounded to the east by the Wasatch fault and to the west by the Great Salt Lake, Oquirrh Mountains, and Utah Lake.

The Wasatch fault is the largest and most hazardous of the faults in the Wasatch Front, capable of producing earthquakes with magnitudes greater than M7. Though the Wasatch fault has not experienced large earthquakes in historic time, the Wasatch Front is active on a microearthquake level (Figure 1) [*Smith and Arabasz*, 1995; *Smith and Sbar*, 1974]. The largest historic earthquake in Utah was the 1934 M_w6.6 Hansel Valley earthquake to the north of the Great Salt Lake [*Doser*, 1990] and persistent activity occurs east and west of the Wasatch fault along nearby Late Quaternary faults.

Yellowstone Volcanic Field GPS Network

The Yellowstone GPS network presently contains 71 permanent stations in the Yellowstone-Snake River Plain (YSRP) and surrounding area (Figure 2, Table S-1). Many of these stations were originally installed and operated by the University of Utah (UU) starting in 1996 under the NSF Continental Dynamics program funding of the Yellowstone Hotspot Geodynamics project. Many other stations were installed by the EarthScope Plate Boundary Observatory (PBO) after 2005. Since 2007, network operations have transitioned to PBO (Figure 3).

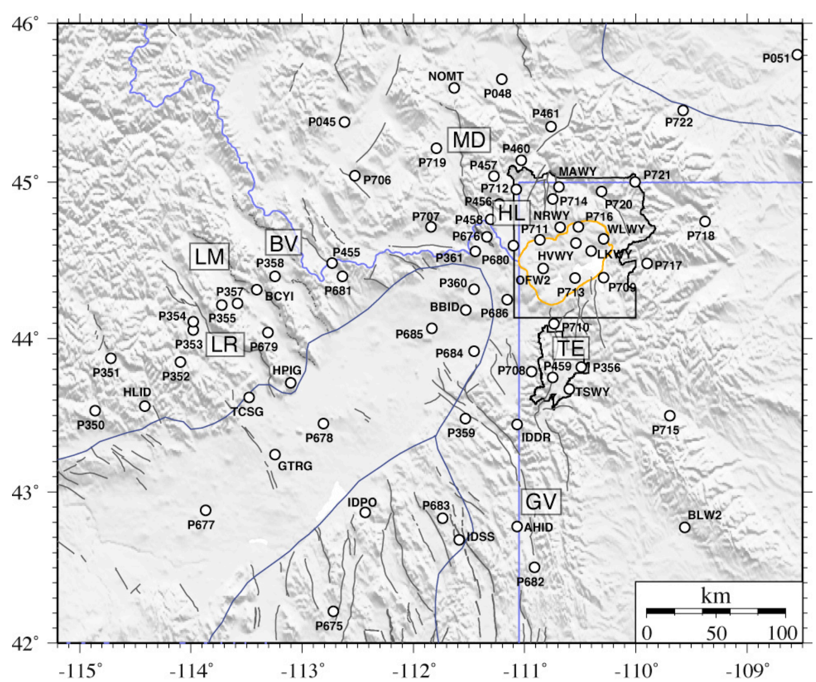

Figure 2. Map of the Yellowstone permanent GPS network. GPS stations are represented by white circles. The Yellowstone caldera is outlined in orange. Abbreviations for major regional faults are: LR=Lost River fault, LM=Lemhi fault, BV=Beaverhead fault, MD=Madison fault, HL=Hebgen Lake fault, TE=Teton fault, and GV=Grand Valley fault. Orange line marks the location of the Yellowstone caldera.

The Yellowstone network measures contemporary deformation in the YSRP and surrounding region. There are several components to the geodetic monitoring: 1) to monitor ongoing deformation of the Yellowstone caldera and characterize volcanic hazards, 2) to identify and characterize episodes of deformation such as the 2004-2009 accelerated uplift [*Chang et al*., 2007; *Chang et al*., 2010] or displacement associated with the 2008-2009 Yellowstone Lake earthquake swarm [*Farrell et al*., 2010], 3) evaluate deformation rates and seismic hazards for large faults around the YSRP, including the Lost River fault, the Hebgen Lake fault , and the Teton fault [*White et al*., 2009], and 4) determine if there is observable deformation and seismic and volcanic hazard associated with the eastern Snake River Plain The permanent Yellowstone GPS network is supplemented by observations recorded at 140 temporary stations in the greater YSRP area.

Field campaigns were performed in 1987, 1989, 1991, 1993, 1995, 2000, and 2003 (Table 1, Table S-2, Figure 4, Figure 5) [*Puskas et al*., 2007]. Additional campaigns in 2008, 2009, and 2010 focused on the Yellowstone caldera, operating 18-25 temporary stations to help resolve ongoing deformation associated with a period of accelerated caldera uplift that started in 2004 and attained uplift rates up to 7 cm/yr [*Change et al.,* 2007] (in contrast to previously measured background values of 1-2 cm/yr of vertical motion). Temporary stations were occupied for at least two days and up to 42 days in each campaign. The network of temporary sites provided densified spatial coverage relative to the permanent network.

Wasatch Fault, Utah, GPS Network

The Wasatch Front GPS network consists of 68 permanent stations distributed across the Wasatch fault in central and northern Utah (Figure 6, Table S-3). These stations are operated by the University of Utah, PBO, and the National Geodetic Survey (NGS). The network began operation in 1997 with 8 stations installed during the first year.

The purpose of the network is to measure the contemporary distribution of deformation across the Wasatch fault. The data are used to estimate slip rates and loading rates of the fault for seismic hazard analysis. Variations in slip rates for different segments of the Wasatch fault are being investigated, with consequent variations in hazard level for different parts of the Wasatch fault. The GPS data are also being examined to identify possible loading on other large regional faults.

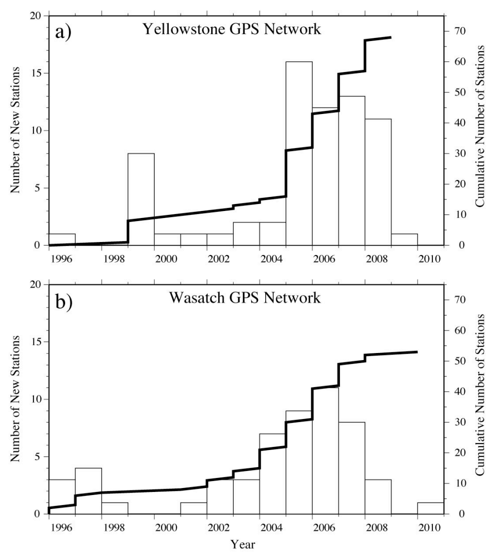

Figure 3. History of installation of new stations for: a) the Yellowstone GPS network and b) the Wasatch GPS network. Heavy dark lines represent the cumulative number of stations in the network.

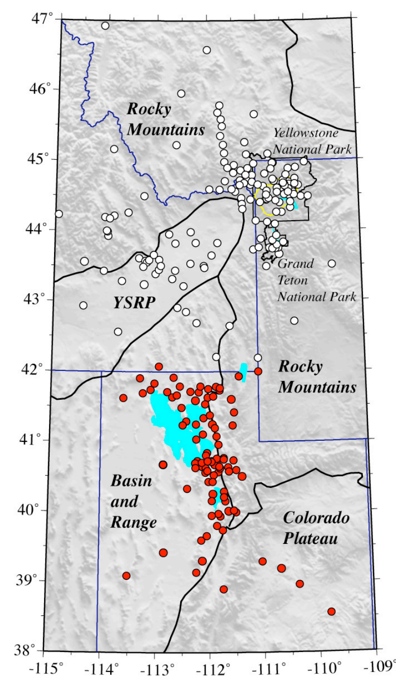

Figure 4. Distribution of temporary GPS station in the Yellowstone hotspot network (white circles) and Wasatch fault network (red circles).

The University of Utah has pioneered the use of GPS to measure deformation of the Wasatch as a proxy for fault loading in a Probabilistic Seismic Hazard Assessment (PSHA) described in *Chang et al*. [2002]. This study was very important for demonstrating the use of GPS observations in area of low contemporary seismicity but high Late Quaternary fault slip rate that characterizes this area of the Basin-Range.

The Wasatch fault permanent GPS network has been supplemented by field campaigns at established surveyor benchmarks. There are 93 stations in the temporary network, and each site typically had measurements taken over a period of two days or more during each campaign (Table 1, Table S-4). Field campaigns were conducted in 1992, 1993, 1994, 1995, 1999, and 2001 [*Chang*, 2004; *Martinez et al*., 1998].

Table 1. List of University of Utah Yellowstone and Wasatch fault GPS field campaigns.

Year	**Area of Campaign**	**Number of Stations**
1987	Yellowstone-Teton	79
1989	Yellowstone-Teton	66
1991	Yellowstone-Teton	90
1992	Wasatch Front	26
1993	Wasatch Front	46
1993	Yellowstone-Teton	61
1994	Wasatch Front	150
1995	Wasatch Front	41
1995	Greater YSRP region	104
1999	Wasatch Front	43
2000	Greater YSRP region	140
2001	Wasatch Front	5
2003	Yellowstone-Teton	79
2008	Yellowstone caldera	17
2009	Yellowstone caldera	17
2010	Yellowstone-Teton	25

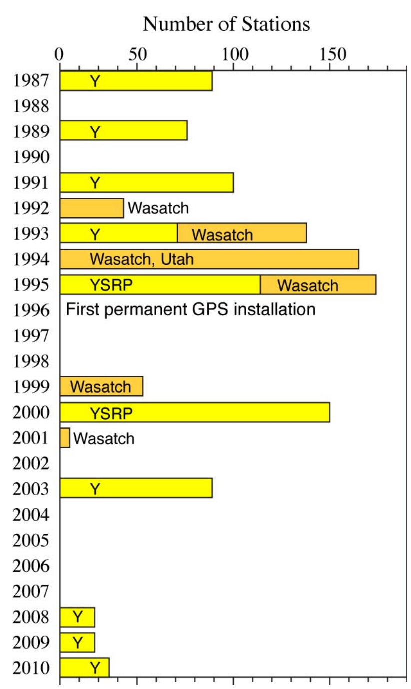

Figure 5. Time distribution of GPS field campaigns. Colored bars represent the number of stations surveyed in a campaign, with Yellow for Yellowstone and orange for Wasatch campaigns.

University of Utah GPS Data Recording

The University of Utah GPS data are recorded at 15 to 30-second intervals in sessions of 8 hours (for campaign stations) to 24 hours (for campaign and permanent stations). The data file for each session is then converted to the Receiver Independent Exchange (RINEX) format, the standard format for processing.

The GPS data are processed using the Bernese GPS software [*Dach et* al., 2007; *Rothacher and Mervart*, 1996] using differential GPS techniques. For a given network, the processing algorithms solve for the daily position of each station. These daily position solutions are combined to obtain the change in position over time, or velocity. For permanent

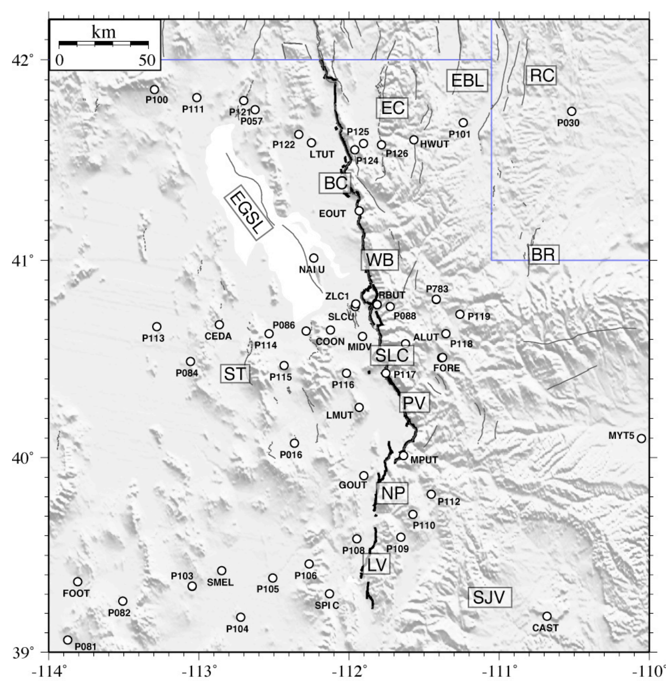

Figure 6. Map of the Wasatch fault, Utah, permanent GPS network, with stations represented by white circles. The Wasatch fault is represented by heavy lines with labeled segments. Other faults are shown by dark gray lines. Labels are: BC=Brigham City segment, WB=Weber segment, SLC=Salt Lake City segment, PV=Provo segment, NP=Nephi segment, LV=Levan segment, EGSL=East Great Salt Lake fault, EC=East Cache fault, EBL=Eastern Bear Lake fault, RC=Rock Creek fault, BR=Bear River fault, and SJV=Southern Joes Valley.

networks, hundreds of days' worth of data are combined. For campaign data, campaigns may be separated by months or years, so only the net change in position is determined.

GPS Satellite Ranging

Satellite ranging, or calculating the distance between a GPS receiver and GPS satellite, is the basis of all GPS processing. Given the known position of at least four satellites and the distance between the satellite and GPS station, it is possible to solve for the three components of the station position (either x, y, z in an earth-centered Cartesian coordinate system, or latitude, longitude, elevation in a spherical coordinate system). In practice there are many sources of errors and biases, from satellite and station clocks, atmospheric effects, satellite position errors, station equipment errors, relativistic effects, random errors, etc. Data processing reduces or eliminates these errors and biases through various analytical and numeric methods, as well as modeling.

The constellation of navigation satellites orbiting the Earth is the basis of the Global Positioning System. The GPS satellites broadcast two carrier signals, generally referred to as L_1 and L_2, with wavelengths of λ_1=19 cm and λ_2=24.4 cm [*Dach et al.*, 2007]. The carrier signals are modulated by two pseudo-random codes and a navigation message. The navigation message contains information on the satellite clock, health, and orbit. The two pseudo-random codes are called the P-code and C/A-code, or precise and coarse-acquisition code, respectively. These codes contain sequences of pseudo-random noise, with unique segments of code assigned to each satellite. The P-code has frequency 10 times that of the C/A-code, with a consequent increase in precision by a factor of 10. Both the P and C/A-codes have lower frequencies than the carrier frequencies.

Satellite positions at any given time are required to obtain the station position. The broadcast orbit data are real-time but only accurate to ~2 m, and greater precision is required for geodetic network monitoring. Instead, precise orbits from the International GNSS Service (IGS) are downloaded from the IGS data center [*Dow et al.*, 2009]. The IGS produces orbit solutions that are accurate to less than 5 cm, the files are released with a latency of ~10 days.

The distance between a satellite and a receiver is known as the range. However, biases and errors will limit the precision to which the range can be determined, and what is actually measured is called the pseudorange. The pseudorange can be calculated from either the broadcast codes or the phase of the carrier signals.

The code pseudorange is obtained by multiplying the travel time by the speed of light to get the distance between satellite and receiver. The receiver generates a P or C/A-code sequence and compares it to the signal received from a satellite. The time offset between the two codes is equal to the travel time.

The phase pseudorange is calculated by solving for the integer number of cycles of the carrier wave between the satellite and receiver. The integer number of cycles is known as the phase ambiguity. The receiver actually measures the fractional phase at the time of signal reception and counts the number of cycles since the satellite was first observed, i.e., the receiver tracks the change in position of the satellite. Multiplying the phase ambiguity plus the fractional phase by the wavelength will give the total distance to the satellite. The phase ambiguity cannot be calculated directly but must be solved for using linear combinations of multiple observations over time or eliminated using differencing techniques.

The precision of the pseudorange measurements depend on the frequency of the signal used as the basis of the measurement [*Wells et al.*, 1986; *Hofmann-Wellenhof et al.*, 1992]. For code pseudoranges based on the P and C/A codes, the predicted precision values are approximately 30 cm and 3 m, respectively. For the phase pseudoranges based on the L1 and L2 carrier signals, the precision would be 2 mm and 2.4 mm, respectively.

Future developments in navigation technology will lead to improved precision over the coming years. The original GPS satellites are operated by the U.S. Department of Defense, but other nations are planning or have launched new satellites. These satellites will broadcast on different frequencies, opening new possibilities for processing. The GLONASS constellation, launched by the Russian Federation Ministry of Defense, is already operational, while the European Space Agency's Galileo satellites and China's Compass satellites will be launched over the next decade. Although the new satellites have or will have different orbital parameters and broadcast signals, the underlying mathematical principles for calculating receiver positions will remain the same.

Differential GPS Processing

The University of Utah uses the techniques of differential GPS to attain the level of precision required for scientific analysis. Ground deformation rates in the Yellowstone and Wasatch networks range from less than 1 mm/yr to several cm/yr, necessitating careful processing to resolve the lower velocities.

The purpose of differential GPS processing is to use various linear combinations and numerical techniques to reduce or eliminate biases and errors where possible. For smaller networks with baselines of tens of kilometers (less than ~30 km), there will be little variation in atmospheric refraction over the network area, so the atmospheric errors will be approximately the same at all stations. Each station will have its own receiver clock error, and each satellite will have it own satellite clock and position errors.

Zero differences are basic pseudorange estimates with clock errors, troposphere and ionosphere errors, and, in the case of phase observations, the phase ambiguities. Single differences are the differences between two stations observing the same satellite at the same time, i.e., baselines. Double differences are computed by subtracting two single difference observations for two different satellites. Double differencing will eliminate satellite clock errors and reduce receiver clock errors. Triple differences are computed by taking double differences at different time epochs. Assuming that the receivers did not lose lock with the satellite between the two time epochs, the triple differencing will eliminate phase ambiguities and troposphere errors. Various combinations of the double difference observations are used during processing to solve for phase ambiguities, ionospheric delays, and tropospheric models.

GPS processing begins with the downloading of data files (Figure 7). Data files include GPS RINEX observation files, precise orbit files, satellite clock files, and earth rotation parameters. Data files are imported into the Bernese format. Receiver clock errors are calculated from code observations and satellite orbit and clock data. Single-difference baselines are formed and checked for outliers and other problems. Double differences are formed, and the Bernese code estimates the station coordinates along with various biases and the phase ambiguities.

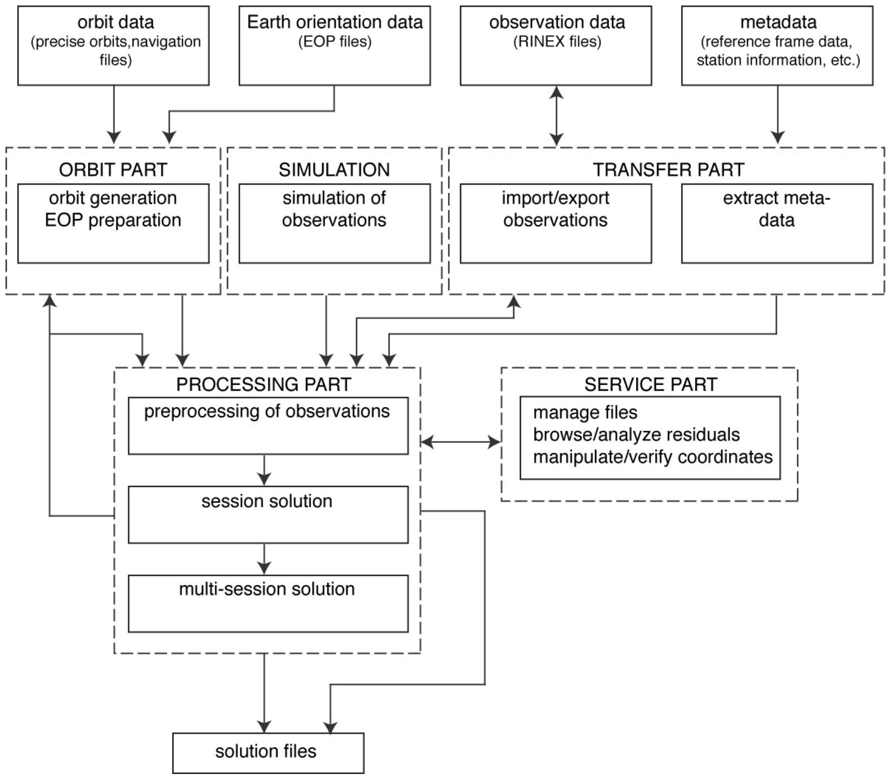

Figure 7. Flow chart illustrating the different steps in Bernese GPS processing (modified from *Dach et al*., 2007).

GPS Data Products

The GPS processing outputs daily position solutions along with relevant statistical data. The daily coordinates typically have uncertainties less than 1 mm for the horizontal components and less than 2 mm in the vertical component (Figure 8).

Earthquake and volcano hazard analysis and research require the change in position of the ground with time, i.e., the ground velocity. Station velocities are estimated separately from the daily solutions. The daily position solutions for all the stations in a network are all correlated and in the same reference frame because they were processed together with differential techniques, but each day is processed independently of the previous day.

To rigorously combine multiple days, each day's network solution must be transformed into the same reference frame through a Helmert transformation. In the Helmert transformation, uniform rotations, translations, and scaling factors are applied to all stations in the network for one day to bring the network into the desired reference frame. The reference frame is defined by reference stations whose coordinates and velocities are known *a priori*. For the permanent network data, the reference stations are typically IGS stations in a global reference frame such as ITRF2000 [*Calais et al*., 2006], ITRF2005 [*Altamimi et al*., 2007], or Stable North America [*Blewitt et al*., 2005]. Campaign network data before ~2000 used local reference frames or an earlier version of the Stable North America reference frame [*Bennett et al*., 2001]. The Stable North America reference frame is frequently used in studies of western U.S. deformation, and holds the interior of the North America continent (i.e., North America east of the Rocky Mountains) fixed so that deformation is with respect to the fixed interior.

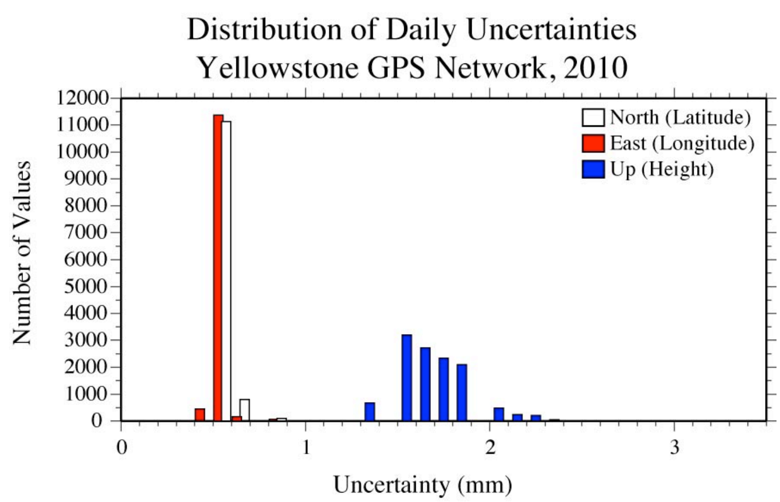

Figure 8. Distribution of errors for components of station positions for all stations in the Yellowstone permanent GPS network in 2010 (January 1 – June 30). Colored bars represent the number of times a particular value or uncertainty was obtained for each component. The latitude (north) component is white, the longitude (east) component is red, and the vertical (up) component is blue. Uncertainties are given to the nearest 0.1 mm, but bars are scaled smaller to show north and east components.

Once the daily solutions are all in the same reference frame, the velocity of each station can be estimated through a weighted least squares fit [*Brockmann*, 1996]. The station velocities give the magnitude and direction of ground motion in the Wasatch Front and the YSRP (Figure 9).

Strain rates are a measure of the change in velocity over a geographical area and are generally interpolated from the velocity data [*Haines and Holt*, 1993; *Shen et al.*, 1996]. The interpolations determine strain on a grid, where each grid square is assumed to deform homogeneously. High strain rates are associated with regions of active deformation, particularly active fault zones and volcanoes (Figure 10).

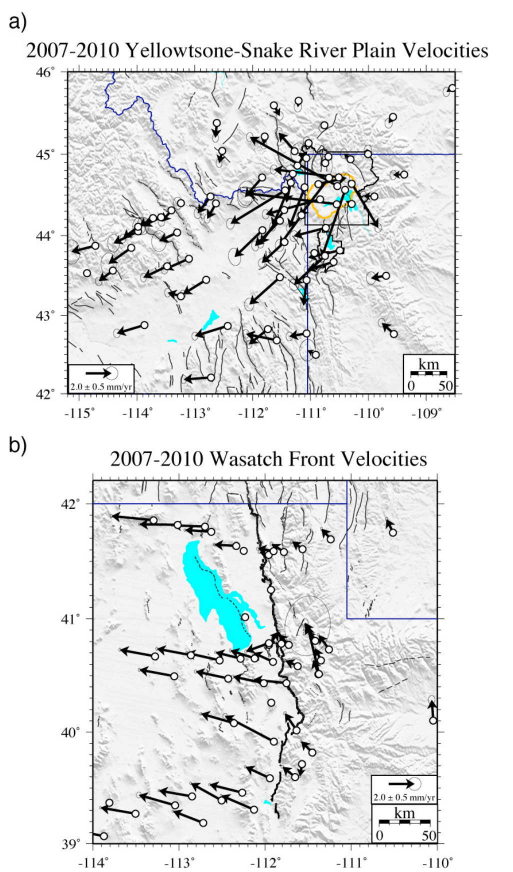

Figure 9. Velocity fields of a) the Yellowstone-Snake River Plain region and b) the Wasatch Front.

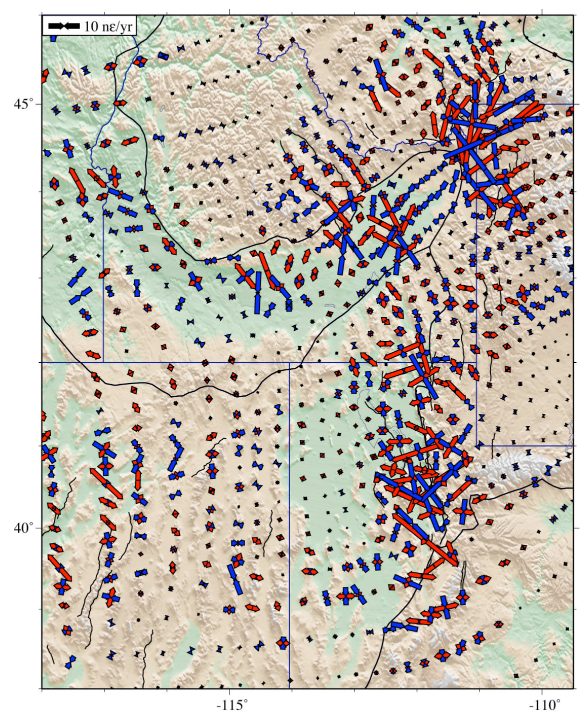

Figure 10. Strain rates of the Yellowstone-Snake River Plain and Wasatch fault zone from *Puskas* [2009]. Blue arrows represent contraction and red arrows represent extension in parts per billion.

The combination of daily solutions in the velocity estimate will produce a single set of coordinates for the stations in the network. The residuals with respect to the combined coordinate solutions can be plotted in a time series as an alternate way to represent change in position over time (Figure 11). The velocity calculations assume a constant rate at the station for a given time period. This assumption is generally true in non-volcanic settings over long time periods of many years [*Langbein*, 2008], but short-term fluctuations can bias velocities at stations operating for less than 2-3 years. Such short-term fluctuations from seasonal water cycles, earthquakes, or volcanic activity can be identified from time series data.

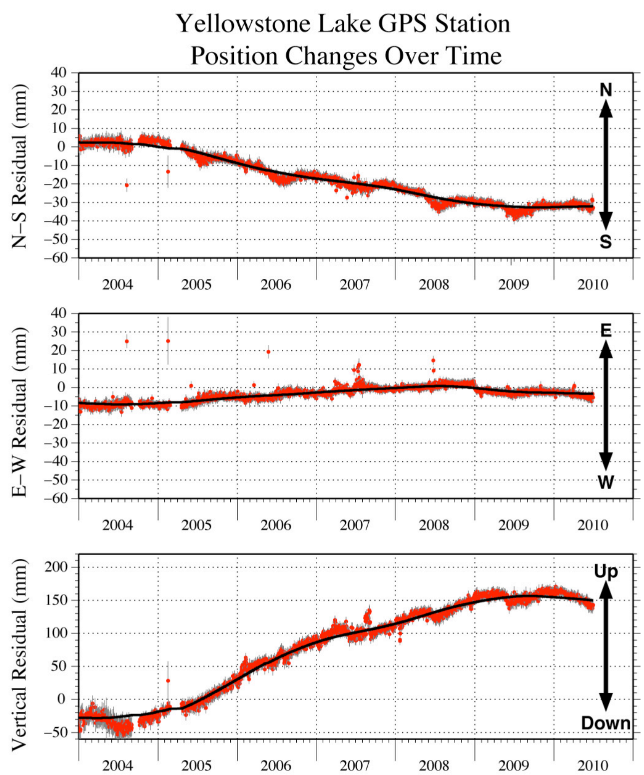

Figure 11. Example of GPS coordinate time series for station at the Lake Junction (LKWY) in Yellowstone National Park showing the change in position over time. The time series reveals the accelerated uplift of the Yellowstone caldera beginning in 2004 and ending in 2009 [*Chang et al.*, 2007]. The red points represent the daily position change and the black lines represent the filtered deformation trend.

The University of Utah Seismology and Active Tectonics Research Group posts station velocities for the Wasatch network and Yellowstone network to their web site. Time series of individual stations' position changes are also available for the Yellowstone and Wasatch regions. Additionally, PBO (GAMIT) and the USGS (Gypsy) processes most of the University of Utah stations and posts them daily. These organizations use different processing software and provide comparisons with our Bernese-determined solutions.

Analysis of GPS Time Series

The time series of individual stations are analyzed for temporal variations, frequency content, and noise characteristics. In addition, GPS time series are affected by white and colored noise [*Langbein*, 2008; *Mao et al*., 1999] that is related to GPS monument stability and local site and atmospheric effects. The time series also contain geologically related low-frequency signals with periods ranging from months to years (Figure 12). The low-frequency signals can be related to magmatic processes [*Chang et al*., 2007; *Chang et al*., 2010], post-seismic deformation [*Chang and Smith*, 2010], co-seismic deformation [*Farrell et al*., 2010], or hydrologic loading. Much of the research at the University of Utah is focused on the Yellowstone caldera as well as earthquake behavior, so the ability to distinguish between contributing sources of deformation is important.

Over long time periods of several (>3-5) years, GPS-derived velocities will generally average out to long-term rates (Figure 13). However, data from stations for shorter time periods are subject to noise and seasonal variations that may bias velocity calculations. Seasonal variations (Figure 13) are generally related to hydrological processes such as groundwater recharge and discharge in aquifers, surface water flow, and snow and lake loading.

These cycles depend on annual precipitation, how much of the precipitation is stored as snowpack over the winter, and the rate at which meteoric water enters the groundwater system or lakes and reservoirs.

GPS position time series can be converted to velocity time series by taking the time derivative. This is done by using a least-squares method to fit the change in deformation in a given time period (Figure 12). The velocity time series are very sensitive to the time window

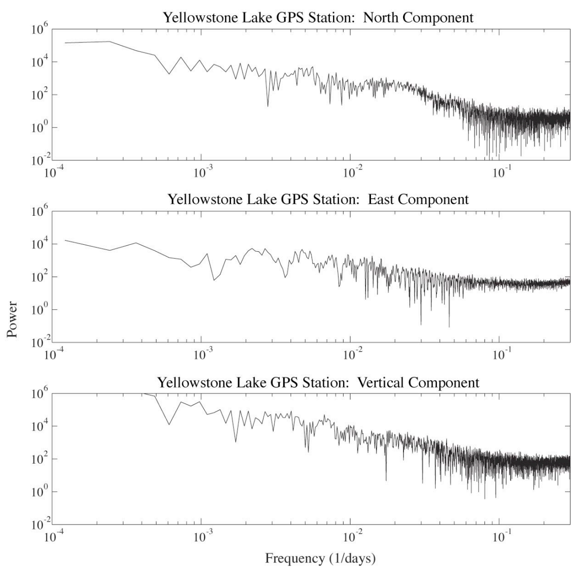

Figure 12. Power spectrum for components of GPS station LKWY at Lake, Wyoming. The power represents the distribution of energy over a range of frequencies. Most of the energy is in the low-frequency signals.

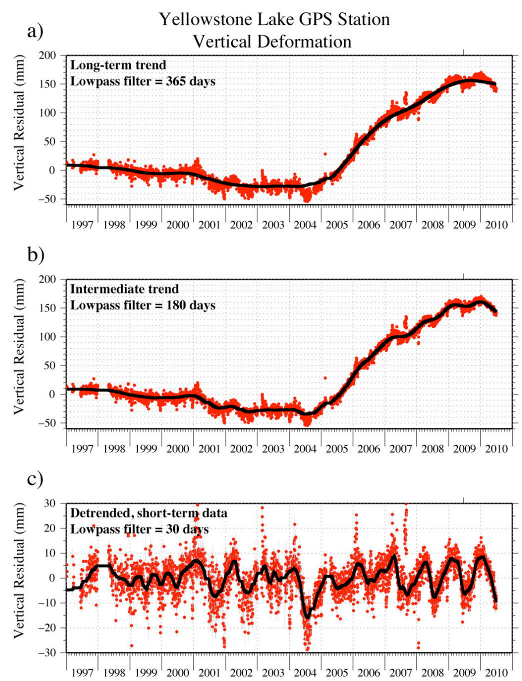

Figure 13. Sample coordinate time series for station LKWY. Black lines represent fitted data that use different parameters: a) long-term trend when deformation signals with periods less than 365 days are removed, b) intermediate trend when signals with periods less than 180 days are removed, and c) short-term deformation from detrended data. The long-term trend was subtracted from the data to get the detrended time series, and the fit was then smoothed with a 30-day lowpass filter.

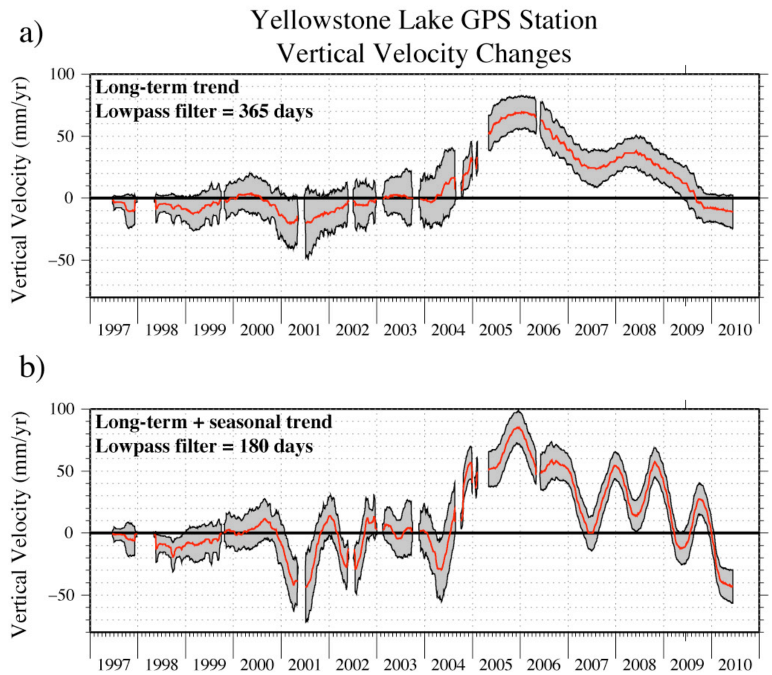

Figure 14. Vertical velocity changes for station LKWY, Wyoming: a) velocities calculated for deformation data filtered with a 1-year lowpass filter, and b) velocities calculated for deformation data filtered with a 6-month lowpass filter. Velocities were taken by calculating the slope of a 30-day time window of the filtered deformation time series (Figure 13).

length and the lowpass filtering parameters used to remove seasonal and other high-frequency motion. Filtering parameters are being analyzed to best constrain the transition from uplift to subsidence in the Yellowstone caldera (Figure 14).

Seasonal Variations in Deformation

One project uses seasonal-trend decomposition [*Cleveland et al*., 1990] and frequency analysis to separate long-term trends into short-term seasonal deformation and long-term trends (Figure 12, 13). Applied to stations in the Yellowstone network, filtering reveals that the seasonal components of deformation (period=365 days) have a peak-to-peak amplitude of up to 2 cm in the vertical component and 0.5-1 cm in the horizontal component. In the Yellowstone caldera peak uplift occurs from winter through spring and maximum subsidence is observed during the summer (Figure 13). Not all stations exhibit regular seasonal deformation.

Hydrologic factors not only affect short-term deformation but can bias long-term measurements as well. Climatic variations in precipitation rates are known to affect lake levels on a decadal scale, and groundwater dynamics can be similarly affected. In populated and agricultural areas, groundwater pumping is known to cause permanent subsidence that can continue for many years after pumping has ceased [*Galloway et al*., 1999].

Groundwater pumping is expected to affect the Wasatch Front, where there are numerous wells in the various valleys, but not the Yellowstone Plateau, where there is minimal infrastructure development. Deformation response to hydrologic changes also depends on the characteristics of the regional aquifers. Groundwater in the Wasatch Front is stored in the unconsolidated sediments of the interconnected, shallow basins of the Basin-Range tectonic province [*Robson and Banta*, 1995]. In Yellowstone, groundwater is stored in basin fill, alluvial deposits, and glacial sediments as well as volcanic rocks [*Whitehead*, 1996].

Real-Time GPS Measurements For Deformation Monitoring and Seismic Recording

The Yellowstone GPS network is being partially updated to real-time streaming by the UNAVCO engineering team and with support from the USGS ARRA funds. In 2010, seven stations will be upgraded to full real-time streaming. The Yellowstone streamed GPS data will be processed for real-time coordinates by the PBO GPS facility then imported into the University of Utah GPS recording facility. Our goal is to employ real-time GPS coordinate data for rapid response in case of earthquake or volcanic activity in Yellowstone as well as importing the processed coordinate data into the University of Utah Seismograph Stations AQMS earthquake recording network, where the data will be treated as seismic coordinate data and integrated into the earthquake analysis.

University of Utah GPS-Related Research Projects

The GPS stations of the University of Utah networks measure ground deformation on the scale of days to years. These data are suitable for examining a range of tectonic and volcanic processes and have been the basis of research projects on the earthquake cycle, Yellowstone magma migration and intrusion, and large-scale intraplate deformation. Recent GPS research projects are summarized in Table 2. The University of Utah and partners have published a number of papers focusing on the YSRP or Wasatch, and many of the more recent papers incorporate GPS data into models of faulting, magmatism, and regional tectonics.

Projects involve studies of magma/volcanic fluid migration [*Chang et al.,* 2010; *Farrell et al*., 2010; *Waite and Smith,* 2002] and earthquakes and related interseismic loading at the Yellowstone Plateau and the Wasatch Front [*Chang and Smith*, 2002; *White et al*., 2009] (Figure 13). The expansion of the EarthScope Plate Boundary Observatory (PBO) GPS network between 2006 and 2008 has supplemented the concomitantly expanding University of Utah networks and allows kinematic analysis of

Table 2. List of recently published University of Utah research papers that incorporate GPS data.

Reference	Subject
Chang and Smith [2002]	Seismic hazards of the Wasatch Front; stress contagion between fault segments
Waite and Smith [2004]	Stress field in the Yellowstone Plateau
Chang et al. [2006]	Deformation of the Wasatch Front
Puskas et al. [2007]	Cycles of deformation in the Yellowstone caldera and regional deformation of the YSRP from 1987 to 2003
Vasco et al. [2007]	Source models of Yellowstone deformation
Chang et al. [2007]	Rapid uplift of Yellowstone caldera starting in 2004
Puskas and Smith [2009]	Block modeling of western U.S. deformation
White et al. [2009]	Seismic hazards of the Teton-Yellowstone region
Farrell et al. [2010	The 2008-2009 Yellowstone Lake earthquake swarm
Chang et al. [2010]	The extraordinary Yellowstone caldera uplift episode, 2004-2010, from GPS and InSAR observations

several large faults including the Wasatch, Teton, and Hebgen Lake faults. The western U.S. deformation data are further being used to constrain regional stress models based on lithospheric structure.

Numerous recent research projects have focused on understanding the relationship between ground deformation and faulting or volcanism. The use of GPS data has helped constrain seismic hazard assessments of the Wasatch fault [*Chang and Smith,* 2002; *Chang et al.,* 2006] and Teton fault [*White et al*., 2009], magma migration and storage in the Yellowstone Plateau [*Chang et al*., 2007; *Vasco et al*., 2007; *Chang et al*., 2010], earthquakes and volcanism in Yellowstone [*Waite and Smith*, 2002; *Farrell et al*., 2010], and regional tectonics and geodynamics [*Waite and Smith,* 2004; *Puskas and Smith*, 2009; *Puskas,* 2009].

Chang and Smith [2002, 2006] integrated GPS data, historic earthquakes, and prehistoric earthquakes to characterize the seismic hazards and kinematics of the Wasatch fault. Their models of stress contagion following large earthquakes and examination of prehistoric earthquakes was consistent with multi-segment ruptures of the Wasatch fault clustered together in time, with earthquakes having characteristic magnitudes of M>6.6. They found GPS-derived slip rates exceeded geologic slip rates derived from past large earthquakes and proposed that aseismic creep may contribute to the discrepancy, or that earthquake loading may be irregular in time. The inclusion of GPS data in the calculation of annual frequencies of exceedence of peak ground acceleration $\geq$0.25 g resulted in an increase in annual frequencies by a factor of 4 compared to the values from historic seismicity only (Figure 15). They also resolved 1.6 ± 0.4 mm/yr extension across the fault, with approximately 50% of the deformation of the 200-km wide eastern Basin-Range tectonic province being concentrated at the Wasatch fault.

Puskas et al. [2007] processed campaign GPS data from 1987 through 2003 in the Yellowstone Plateau and eastern Snake River Plain and identified cycles of uplift and subsidence in the Yellowstone caldera (Figure 16). Deformation sources associated with these cycles were modeled by *Vasco et al*. [2007], who combined GPS velocity data with Interferometric Synthetic Aperture Radar (InSAR) for the periods 1996-2000 (northwest caldera uplift) and 2000-2002 (caldera subsidence). The deformation sources were imaged as inflating or deflating bodies at 6-10 km depths, at the top of the tomographically imaged magma reservoir [*Husen et al*., 2004]. When the Yellowstone caldera began a rapid uplift episode in 2004, *Chang et al*. [2007] similarly used permanent GPS data and InSAR data to model the source as a sill near the top of the magma reservoir (Figure 17). They interpreted the accelerated uplift as the effect of

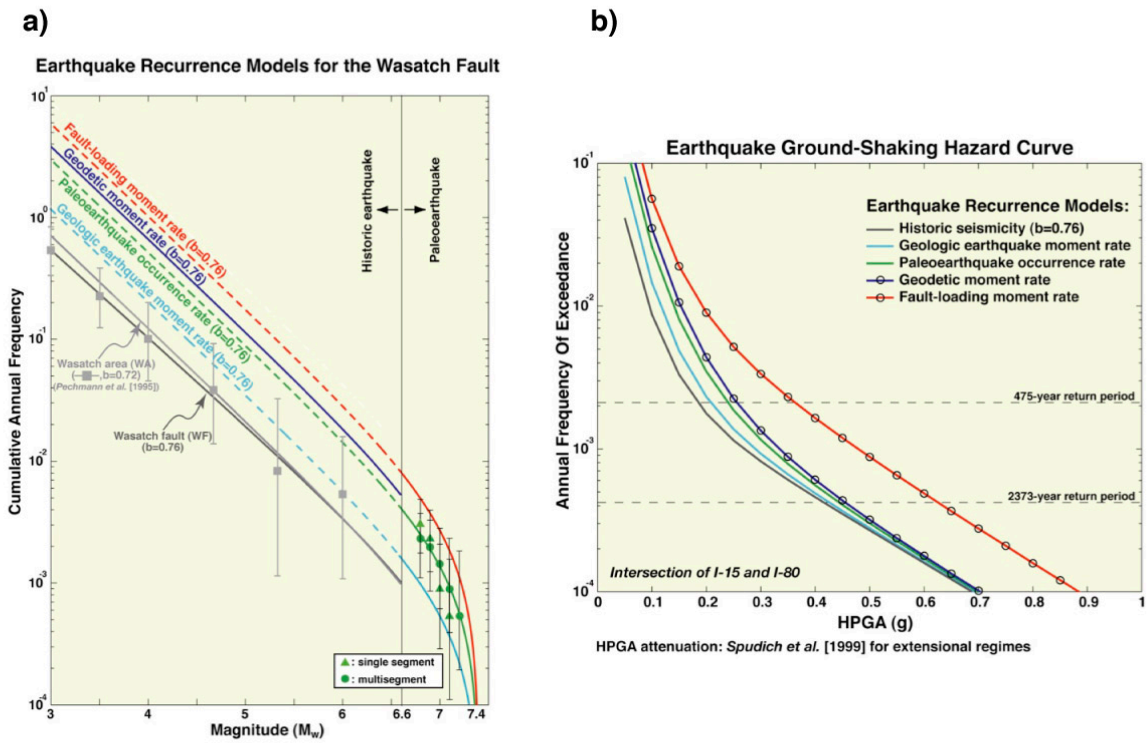

Figure 15. Probabilistic seismic hazard determinations (a) and ground-shaking hazard (b) of the Wasatch fault [*Chang and Smith,* 2002]. The cumulative annual frequency depends on the loading rate of the fault. The loading rate is estimated from historic earthquake rates, prehistoric large earthquake rates, and GPS measurements.

magma recharge in the reservoir and modeled the surface deformation as the result of a volcanic sill (Figure 18).

Puskas and Smith [2009] compiled over 2000 GPS velocity measurements in the western U. S. and used the data to model the kinematics of western U.S. deformation. The southwest motion of the YSRP and westward extension at the Wasatch Front are components of a large-scale rotation of the direction of deformation (Figures 19, 20).

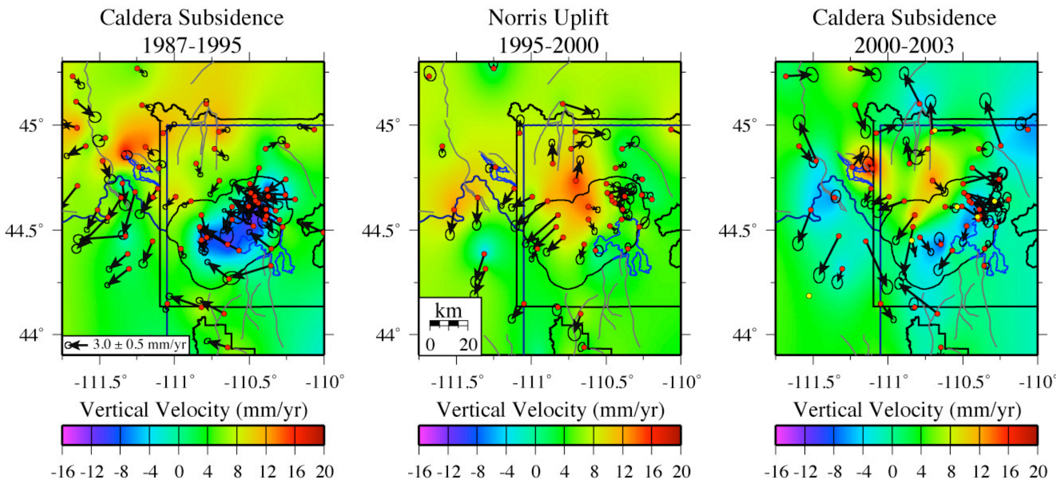

Figure 16. GPS time windows of *Puskas et al*. [2007]. Vectors represent horizontal motion measured during GPS campaigns. Colored backgrounds represent vertical motion.

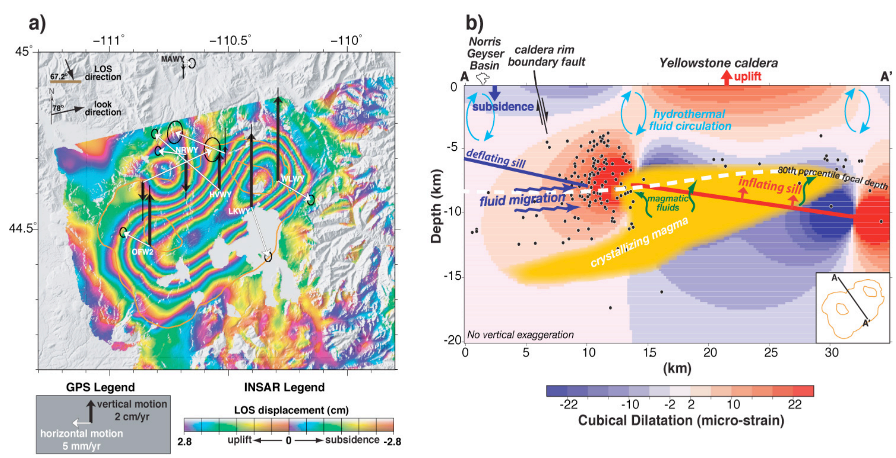

Figure 17. Rapid uplift (a) and sill model at top of magma reservoir (b) of *Chang et al*. [2007]. White vectors represent GPS-measured horizontal motion and black vectors represent GPS-measured vertical motion. The colored background represents near-vertical deformation measured by InSAR interferometry.

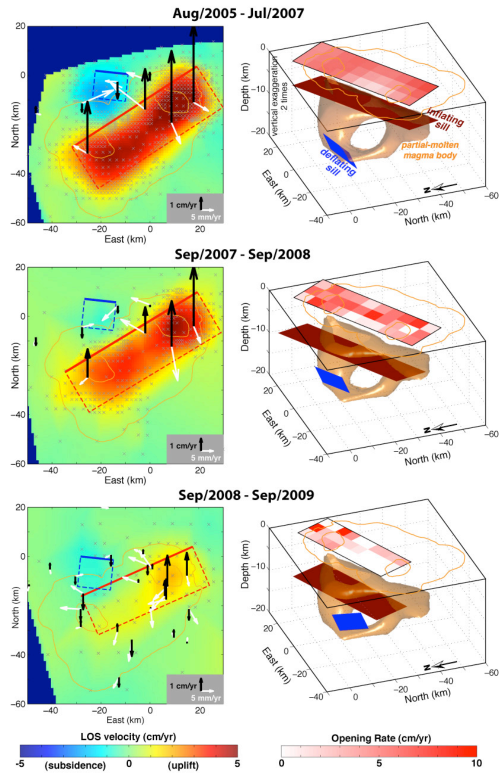

Figure 18. Models of caldera deformation from *Chang et al*. [2010] revealing decreasing uplift rates over time. Deformation sources are represented by red rectangles for uplift and inflation in the caldera (orange outline) and blue rectangles for subsidence and deflation at the northwest caldera boundary. Map view (left column) shows the observed velocities from InSAR as colored background and observed GPS velocities as black and white vectors for vertical and horizontal deformation, respectively. Oblique, 3D view (right column) shows deformation sources relative to the magma reservoir (orange body).

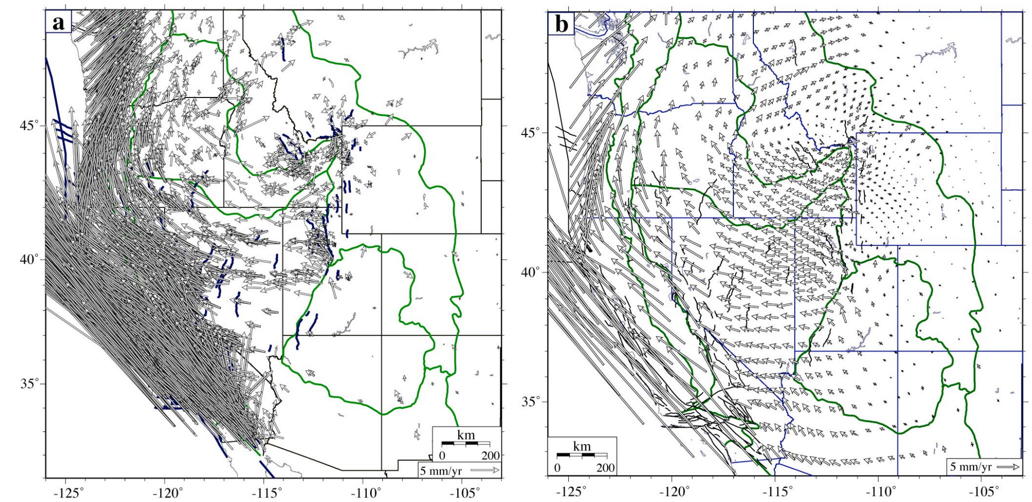

Figure 19. Compilation of western U.S. velocity vectors (a) and interpolated model of deformation (b).

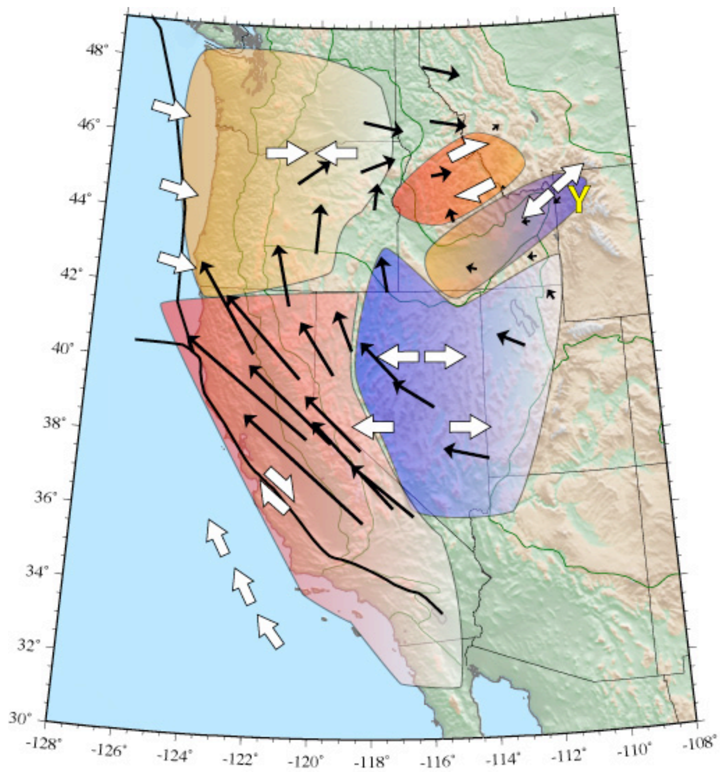

Figure 20. Summary of western U.S. deformation from GPS measurements [*Puskas and Smith* [2009]. Block velocities are shown as black arrows, while the large white arrows indicate the general sense of regional motion and are not to scale. Colored regions highlight deformation types: blue represents extensional domains, red represents shear domains, and orange represents contracting domains.

The pattern of deformation is interpreted as being caused by interplate interactions at the western North America plate boundary, gravitational collapse of the Basin-Range, and stress perturbations from the topographic swell associated with the Yellowstone hotspot. Western U.S. stress modeling [*Puskas,* 2009] indicates that the Yellowstone hotspot swell contributes significantly to regional extension, while plate boundary interactions between the North America tectonic plate and the Juan de Fuca plate in the Cascadia subduction zone and Pacific plate at the San Andreas fault zone also help determine the regional pattern of rotation. Earlier regional stress studies of the YSRP [*Waite and Smith*, 2004] had noted the changes in stress direction associated with the Yellowstone hotspot swell and its importance in western U.S. tectonics.

The Yellowstone topographic swell increases the potential energy by increasing the regional crustal density structure. The gravitational potential energy can be calculated based on topography and lithospheric density structure (Figure 21) [*Puskas,* 2009]. The average horizontal stress field was derived from the gravitational potential energy and constrained by the western U.S. strain rate field (Figure 22). The resulting stress models confirmed the importance of interplate interactions driving rotation in western U.S. deformation, and revealed how the high elevations of the Yellowstone hotspot topographic swell produce regional extension (Figure 23). However, thermal subsidence of the eastern Snake River Plain, combined with magmatic intrusions into the crust, act to reduce the gravitational potential energy and stress magnitudes in the YSRP (Figure 21). The reduced stresses may contribute to the reduced earthquake activity within the Snake River Plain (Figure 1). However, the stress model does not match the strain rate model exactly (Figure 23), and it is hypothesized that combinations of time-dependent deformation, shallow deformation sources, and small-scale variations in the stress field below the model's resolution all contribute variations in the observed GPS velocities and lead to localized misfit with the stress model. Other factors such as coupling of the lithosphere to mantle flow can also lead to misfit, because they are not accounted for in the stress modeling.

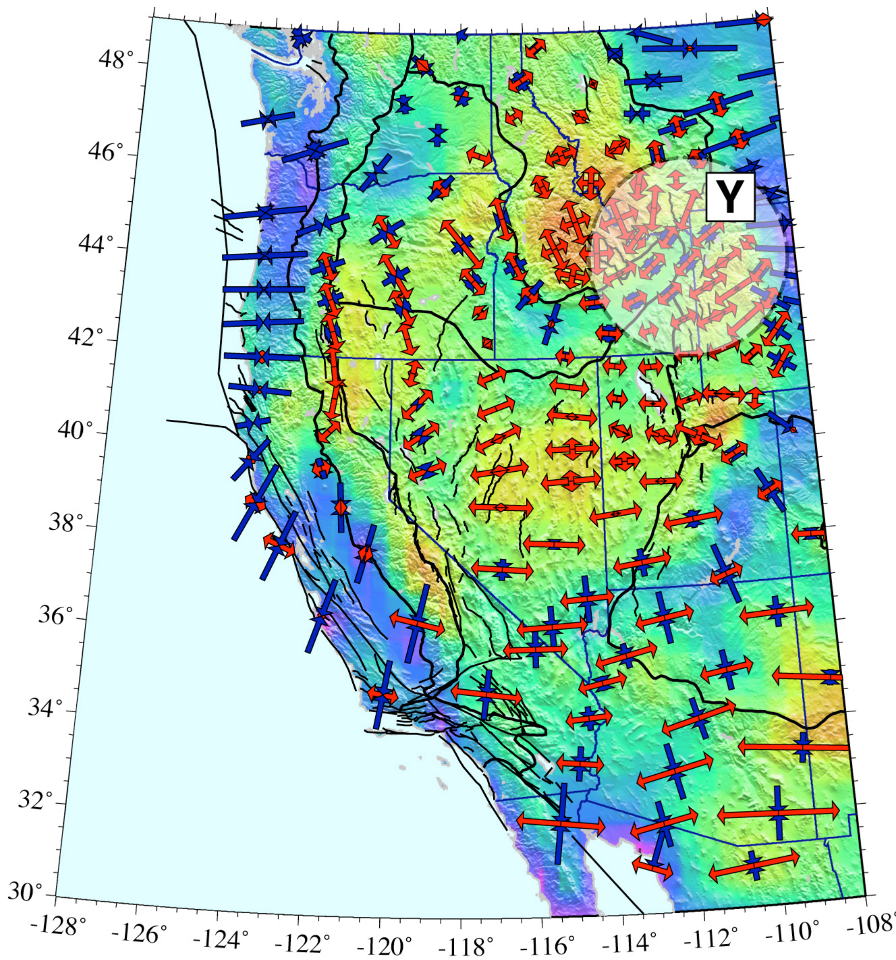

Figure 21. Gravitational potential energy (color background) of the western U.S., with average horizontal stresses in the lithosphere represented by red arrows (tension) and blue arrows (compression). The Yellowstone hotspot swell is marked by the shaded region.

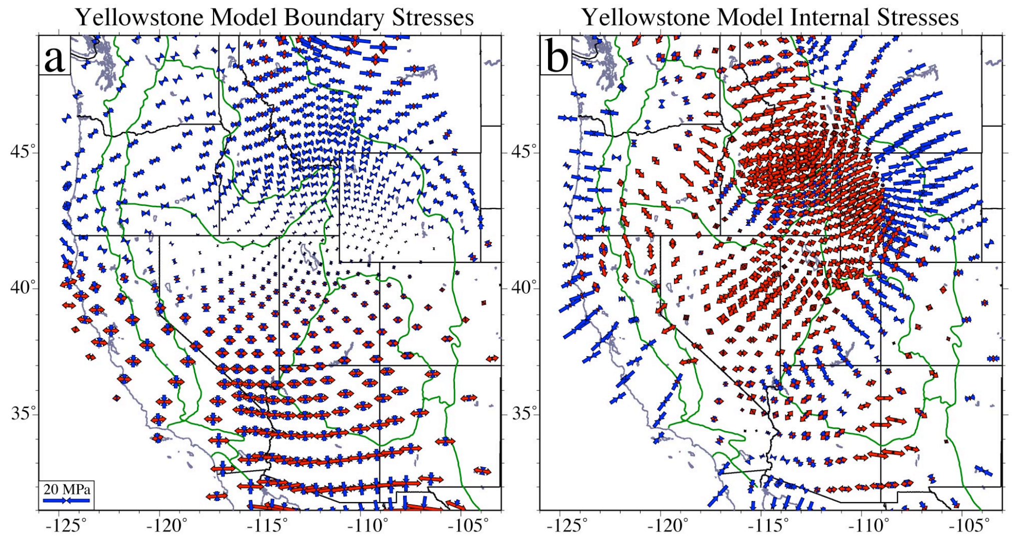

Figure 22. Components of the total stress field (Figure 18): a) boundary stresses derived by matching stress directions to strain rate directions at model area boundaries, and b) internal stresses from topography and lithospheric structure from seismic data [*Puskas*, 2009].

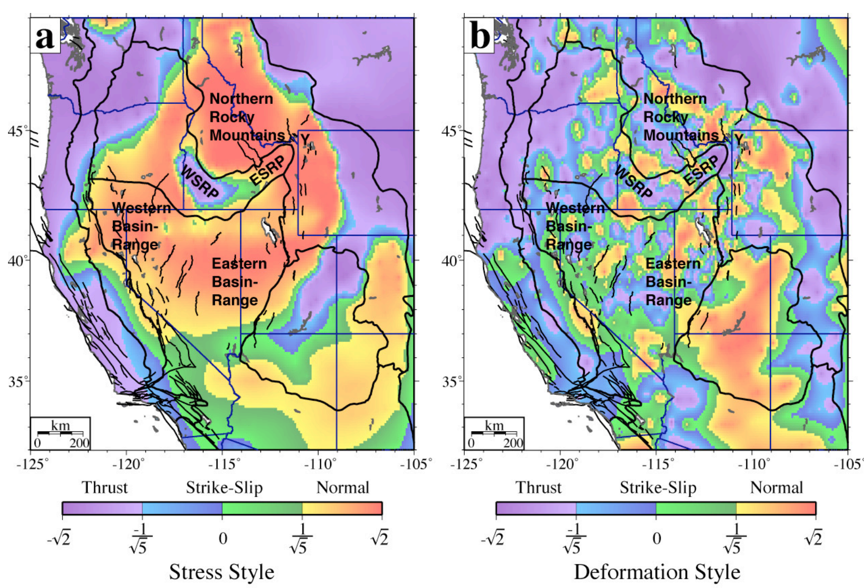

Figure 23. Predicted deformation styles of the western U.S. based on a) stress modeling and b) interpolated strain rates from GPS data [*Puskas*, 2009].

The interaction of the Yellowstone mantle plume with the North America tectonic plate was explored by *Smith et al*. [2009]. This study reveals the importance of Yellowstone's plume as the source driving volcanism of the Columbia flood basalts starting 16 million years ago and then the volcanism of the YSRP. This volcanic activity has altered the topography and lithospheric structure of the YSRP and altered the regional stress field, resulting in volcanic landforms and processes observed today.

Research based on GPS-measured ground motion leads to a better understanding of the processes of faulting and volcanism, and the subsurface structures that are the sources of deformation. With combined seismic data, fault-slip data, other geodetic measurements, it has become possible to model the stresses driving deformation. Furthermore, we can integrate our knowledge of the Wasatch fault and Yellowstone volcanic field into the larger tectonic framework. In this framework, the Wasatch fault is part of a major tectonic boundary between the stable North America plate interior and the rapidly deforming western U.S., while the Yellowstone hotspot is a mantle-derived source of volcanism that has affected deformation rates and directions over a large part of the western U.S.

Acknowledgements

Collaborators in the Yellowstone and Wasatch fault GPS projects included Charles Meertens, Suzette Payne, Ronald Harris, Dan Dzurisin, Anthony Lowry, Henry Heasler and Rob Reilinger. Field and technical assistance was provided by David Drobeck. We appreciate the support for data acquisition of our Yellowstone projects from the National Science Foundation, the U.S. Geological Survey Volcano Hazards Program (Cooperative Agreement #07HQAG0024), Yellowstone and Grand Teton National Parks, the Idaho

National Laboratory, the EarthScope Plate Boundary Observatory, and the Utah Geological Survey. Long-term Yellowstone hotspot research was primarily supported by the NSF Continental Dynamics program grants #EAR 9725431, 0314298, 9725431, and 9316289. The Wasatch fault GPS project was supported by the U.S. Geological Survey NEHRP (National Earthquake Hazard Reduction Program) grants 02HQGR0098, 04HQAG0023, 07HQAG0027, G10AC00159. The University of Utah provided computational support and the University of Utah Seismograph Stations provided engineering support for GPS monitoring. UNAVCO provided GPS instruments for campaign surveys and the EarthScope PBO program has supported the Yellowstone and Wasatch fault continuous GPS networks under the NSF EarthScope Plate Boundary Observatory (EAR-0350028 and EAR-0732947). Support for the UNAVCO equipment and services that we used during the Wasatch and Yellowstone campaigns came from the National Science Foundation and National Aeronautics and Space Administration under NSF Cooperative Agreement EAR-0735156.

The University of Utah originally installed and operated the permanent GPS stations in the Yellowstone and Wasatch GPS networks. After the implementation of the EarthScope program and the installation of the PBO network, most of the university stations have been transferred to PBO (see supplementary material for current status of stations).

References

Altamimi, Z., X. Collilieux, J. Legrand, B. Garayt, and C. Boucher (2007), ITRF2005: A new release of the International Terrestrial Reference Frame based on time series of station positions and earth orientation parameters, *J. Geophys. Res.*, *112*(B9), doi: 10.1029/2007JB004949.

Bennett, R, A., J. L. Davis, J. E. Normandeau, and B. P. Wernicke, (2001), Space geodetic measurements of plate boundary deformation in the western U.S. Cordillera, in *Plate Boundary Zones*, edited by S. Stein and J. Freymueller, pp. 27-55, AGU, Washington, D.C.

Blewitt, G., D. Argus, R. Bennett, Y. Bock, E. Calais, M. Craymer, J. Davis, T. Dixon, J. Freymueller, T. Herring, D. Johnson, K. Larson, M. Miller, G. Sella, R. Snay, M. Tamisiea, (2005), A Stable North American Reference Frame (SNARF): First Release, Proceedings of the Joint UNAVCO/IRIS Workshop, Stevenson, WA, USA, June 9–11.

Brockmann, E. (1996), Combination of solutions for geodetic and geodynamic applications of the Global Positioning System (GPS), Ph.D dissertation, 211 pp., University of Bern, Bern, Switzerland.

Byrd, J.O.D., R.B. Smith, and J.W. Geissman, (1994), The Teton Fault, Wyoming: topographic signature, neotectonics and mechanisms of deformation, *J. Geophys. Res.*, 99, 20,095-20,122.

Calais, E., J. Y. Han, C. DeMets, and J. M. Nocquet, (2006), Deformation of the North American plate interior from a decade of continuous GPS measurements, *J. Geophys. Res.*, 111, B06402, doi:10.1029/2005JB004523.

Chang, W. L., (2004), GPS (Global Positioning System) studies of the Wasatch Fault Zone, Utah, with implications for elastic and viscoelastic fault behavior and earthquake hazard, Ph.D dissertation, 201 pp., University of Utah, Salt Lake City, Utah.

Chang, W. L., and R. B. Smith, (2002), Integrated seismic-hazard analysis of the Wasatch Front, Utah, *Bull. Seis. Soc. Am.*, 92(5), 1904-1922.

Chang, W. L., and R. B. Smith, (2010), Lithospheric rheology from postseismic deformation of a M=7.5 normal-faulting earthquake with implications for continental kinematics, *unpublished manuscript*.

Chang, W. L., R. B. Smith, C. Wicks, J. Farrell, and C. M. Puskas, (2007), Accelerated uplift and magma intrusion of the Yellowstone caldera, 2004-2006, *Science*, doi: 10.1126/science.1146842.

Chang, W. L., R. B. Smith, C. M. Meertens, and R. A. Harris, (2006), Contemporary deformation of the Wasatch Fault, Utah, from GPS measurements with implications for interseismic fault behavior and earthquake hazard: Observations and kinematic analysis, *J. Geophys. Res.*, 111, B11405, doi: 10.1029/2006JB004326.

Chang, W.L., R. B. Smith, C. Wicks, J. Farrell, and C. M. Puskas, (2010), Magmatic source modeling of temporal variations of high uplift rates in the Yellowstone caldera, 2004-2009, *Geophys. Res. Lett.*, (*in press*).

Christiansen, R. L., (2001), The Quaternary and Pliocene Yellowstone Plateau volcanic field of Wyoming, Idaho, and Montana, *U. S. Geol. Surv. Prof. Pap. 729-G*, 120 pp., U. S. Geol. Surv., Denver, CO.

Christiansen, R. L., J. B. Lowenstern, R. B. Smith, H. Heasler, L. A. Morgan, M. Natenson, L. G. Mastin, L. J. P. Muffler, and J. E. Robinson, (2007), Preliminary assessment of volcanic and hydrothermal hazards in Yellowstone National Park and vicinity, *U. S. Geol. Surv. Open-file Report 2007-1071*, 94 pp., U. S. Geol. Surv., Denver, CO.

Cleveland, R. B., W. S. Cleveland, J. E. McRae, and I. Terpenning, 1990, STL: A seasonal-trend decomposition procedure based on Loess, J. Off. Sta., 6(1), 3-73.

Dach, R., U. Hugentobler, P. Fridez, M. Meindl, (Eds.), (2007), *Bernese GPS Software Version 5.0*, 612 pp., Astronomical Institute Univ. of Berne, Berne, Switzerland.

Dow, J. M., R. E. Neilan, and C. Rizos, (2009), The International GNSS Service in a changing landscape of Global Navigational Satellite Systems, *J. Geod.*, 83, 191-198, doi:10.1007/s00190-008-0300-3.

Farrell, J., S. Husen and R.B. Smith, (2009), Earthquake swarm identification and *b*-value mapping of the Yellowstone volcanic-tectonic system, *J. Vol. Geotherm. Res.*, 188, 260-276, doi:10.1016/j.jvolgeores.2009.08.008.

Farrell, J., R.B. Smith, T. Taira, W.L. Chang, and C.M. Puskas, (2010), Dynamics of the intense 2008-2009 Yellowstone Lake earthquake swarm, *Geophys. Res. Lett.*, (in press).

Galloway, D. I., D. R. Jones, and S. E. Ingebritsen, (1999), Land subsidence in the United States, *U.S. Geol. Surv. Circular* 1182, 177p.

Haines, A. J., and W. E. Holt, (1993), A procedure for obtaining the complete horizontal motions within zones of distributed deformation from the inversion of strain rate data, *J. Geophys. Res.*, 98(B7), 12,057-12,082.

Hofmann-Wellenhof, B., H. Lichtenegger, and J. Collins, (1992), *Global Positioning System: Theory and Practice*, 2nd ed., 326 pp., Springer-Verlag, New York.

Husen, S., R. B. Smith, and G. P. Waite, (2004), Evidence for gas and magmatic sources beneath the Yellowstone volcanic field from seismic tomographic imaging, *J. Volc. and Geotherm. Res.*, *131*, 397-410, doi:10.1016/S0377-0273(03)00416-5.

Langbein, J., (2008), Noise in GPS displacement measurements from Southern California and Southern Nevada, *J. Geophys. Res.*, 113, B05405, doi: 10.1029/2007JB005247.

Mao, A., C. G. A. Harrison, and T. H. Dixon, (1999), Noise in GPS coordinate time series, *J. Geophys. Res.*, 104(B2), 2797-2816.

Martinez, L., C.M. Meertens, and R.B. Smith, (1998), Rapid deformation rates along the Wasatch fault zone, Utah, from first GPS measurements with implications for earthquake hazard, *Geophys. Res. Lett.*, 25, 567-570.

Pechmann, J. C., and W. J. Arabasz, (1995), The problem of the random earthquake in seismic hazard analysis: Wasatch Front region, Utah, in *Environmental and Engineering Geology of the Wasatch Front Region: 1995 Symposium and Field Conference*, W. R. Lund (Editor), Utah Geol. Assoc., 77-93.

Puskas, C. M., (2009), Contemporary deformation, kinematics, and dynamics of the Yellowstone hotspot and western U.S interior from GPS, fault slip rates, and earthquake data, Ph.D dissertation, 368 pp., University of Utah, Salt Lake City, Utah.

Puskas, C. M., and R. B. Smith, (2009), Intraplate Deformation and Microplate Tectonics of the Yellowstone Hotspot and Surrounding Western U.S. Interior, *J. Geophys. Res.*, 114, B04410, doi:10.1029/2008JB005940.

Puskas, C. M., R. B. Smith, C. M. Meertens, and W. L. Chang, (2007), Crustal deformation of the Yellowstone-Snake River Plain volcanic system: campaign and continuous GPS observations, 1987-2004, *J. Geophys. Res.*, 112, B03401, doi:10.1029/2006JB004325.

Robson, S. G., and E. R. Banta, (1995), Ground water atlas of the United States Arizona, Colorado, New Mexico, Utah, *U.S. Geol. Surv. Hydrological Investigations Atlas*, HA 730-C.

Rothacher, M., and L. Mervart (Eds.) (1996), *Bernese GPS Software Version 4.0*, 418 pp., Astronomical Institute Univ. of Berne, Berne, Switzerland.

Shen, Z. K., D. D. Jackson, B. X. Ge, (1996), Crustal deformation across and beyond the Los Angeles basin from geodetic measurements, *J. Geophys. Res.*, *101*, 27,957-27,980.

Smith, R. B., and W. J. Arabasz, (1991), Seismicity of the Intermountain Seismic Belt, in Neotectonics of North America, edited by D.B. Slemmons, E.R. Engdahl, M.D. Zoback, and D.D. Blackwell, pp. 185-228, Geological Survey of America.

Smith, R. B., and L. W. Braile, (1994), The Yellowstone hotspot, *J. Volc. and Geotherm. Res.*, 61, 121-187.

Smith, R. B., and M. L. Sbar, (1974), Contemporary tectonics and seismicity of the western United States with emphasis on the Intermountain Seismic Belt, *Geol. Soc. Am. Bull.*, *85*, 1205-1218.

Smith, R.B., M. Jordan, B. Steinberger, C. Puskas, J. Farrell, G. P. Waite, S. Husen, W. Chang, and R. O'Connell, (2009), Geodynamics of the Yellowstone hotspot and mantle plume: Seismic and GPS imaging, kinematics, mantle flow, *J. Volc. and Geotherm. Res.*, 188(103), 26-65, doi:10.1016/j.jvolgeores.2009.08.020.

Spudich, P., J., W. B. Joyner, A. G. Lindh, D. M. Boore, B. M. Margaris, and J. B. Fletcher, (1999), SEA99: A revised ground motion prediction relation for use in extensional tectonic regimes, *Bull. Seismol. Soc. Am.* 89, 1156-1170.

Vasco, D. W., C. M. Puskas, R. B. Smith, and C. M. Meertens, (2007), Crustal deformation and source models of the Yellowstone volcanic field from geodetic data, J. Geophys. Res., 112, B07402, doi:10.1029/2006JB004641.

Waite, G. P., and R. B. Smith, (2002), Seismic evidence for fluid migration accompanying subsidence of the Yellowstone caldera, *J. Geophys. Res.*, *107(B9)*, 2177, doi: 10.1029/2001JB000586.

Waite, G. P., and R. B. Smith, (2004), Seismotectonics and stress field of the Yellowstone volcanic plateau from earthquake first-motions and other indicators, *J. Geophys. Res.*, 109, B02301, doi:10.1029/2003JB00267.

Wells, D. E., N. Beck, D. Delikaraoglou, A. Kleusberg, E. J. Krakiwsky, G. Lachapelle, R. B. Langley, M. Nakiboglu, K. P. Schwartz, J. M. Tranquilla, and P. Vanicek, (1986), *Guide to GPS Positioning*, Canadian GPS associates, Fredericton, N.B., Canada.

White, B. J. P., R. B. Smith, S. Husen, J. Farrell and I. Wong, 2009, Seismicity and earthquake hazard analysis of the Teton-Yellowstone region, Wyoming, , J. *Vol. Geotherm. Res*, 188, 277-296, doi:10.1016/j.jvolgeores.2009.08.015.

Whitehead, R. L., (1996), Ground water atlas of the United States Montana, North Dakota, South Dakota, Wyoming, *U.S. Geol. Surv. Hydrological Investigations Atlas*, HA 730-*C*.

Supplemental Material

This section contains GPS station coordinate lists from the University of Utah's permanent networks and campaign networks.

Table S-1. Permanent GPS Stations in the Yellowstone Network.

Station	Longitude	Latitude	Operating Agency
AHID	-111.064	42.773	PBO
BBID	-111.526	44.185	PBO
BCYI	-113.406	44.316	PBO
BLW2	-109.558	42.767	PBO
BLWY[a]	-109.558	42.767	PBO
GTRG	-113.241	43.244	PBO
HLID	-114.414	43.563	PBO
HPIG	-113.100	43.713	PBO
HVWY	-110.536	44.614	PBO
LKWY	-110.400	44.565	PBO
MAWY	-110.689	44.973	PBO
NOMT	-111.630	45.597	PBO
OFW2	-110.831	44.451	PBO
OFWY[a]	-110.832	44.452	PBO
NRWY	-110.678	44.715	PBO
TCSG	-113.478	43.619	PBO
TSWY	-110.597	43.674	PBO
WLWY	-110.287	44.640	PBO
P045	-112.617	45.383	PBO
P048	-111.204	45.653	PBO
P051	-108.546	45.807	PBO
P351	-114.719	43.874	PBO
P352	-114.096	43.849	PBO
P353	-113.979	44.055	PBO
P354	-113.979	44.109	PBO
P355	-113.722	44.218	PBO
P356	-110.489	43.817	PBO
P357	-113.582	44.227	PBO
P358	-113.241	44.402	PBO
P359	-111.529	43.482	PBO
P360	-111.451	44.318	PBO
P361	-111.440	44.560	PBO
P455	-112.729	44.486	PBO
P456	-111.225	44.863	PBO
P457	-111.273	45.041	PBO
P458	-111.302	44.766	PBO
P459	-110.746	43.748	PBO

Table S-1. Continued.

Station	Longitude	Latitude	Operating Agency
P460	-111.029	45.140	PBO
P461	-110.759	45.354	PBO
P675	-112.719	42.212	PBO
P676	-111.338	44.654	PBO
P677	-113.868	42.879	PBO
P678	-112.805	43.449	PBO
P679	-113.306	44.040	PBO
P680	-111.099	44.598	PBO
P681	-112.636	44.400	PBO
P682	-110.908	42.503	PBO
P683	-111.735	42.827	PBO
P684	-111.450	43.919	PBO
P685	-111.830	44.068	PBO
P686	-111.155	44.252	PBO
P686	-111.155	44.252	PBO
P706	-112.524	45.043	PBO
P707	-111.837	44.719	PBO
P708	-110.934	43.786	PBO
P709	-110.286	44.392	PBO
P710	-110.732	44.096	PBO
P711	-110.861	44.636	PBO
P712	-111.072	44.957	PBO
P713	-110.544	44.390	PBO
P714	-110.744	44.896	PBO
P715	-109.690	43.501	PBO
P716	-110.512	44.718	PBO
P717	-109.897	44.485	PBO
P718	-109.376	44.753	PBO
P719	-111.789	45.218	PBO
P720	-110.306	44.943	PBO
P721	-110.002	45.003	PBO
P722	-109.571	45.457	PBO
IDPO	-112.432	42.866	NGS
IDSS	-111.584	42.686	NGS
IDDR	-111.064	43.445	NGS
IDPO	-112.432	42.866	NGS
IDSS	-111.584	42.686	NGS
IDDR	-111.064	43.445	NGS

[a]Station has been retired and is no longer operating.

Table S-2. Temporary stations from the Yellowstone-Snake River Plain field campaigns.

Station	Longitude	Latitude
1404	-110.635	44.267
5223	-113.193	43.558
0026	-113.841	44.223
0A37	-113.202	43.564
0Z36	-113.222	43.579
10RD	-110.614	44.612
16EM	-116.466	42.656
25MD	-110.486	44.678
32FM	-113.677	43.292
A047	-109.571	43.511
A162	-110.787	45.102
ABDI	-112.471	43.223
AECU	-112.950	43.595
AIRP	-111.111	44.700
AIRP	-111.853	41.787
ANDR	-114.024	44.198
ARBE	-110.439	44.631
B118	-113.264	43.496
BAIR	-112.064	41.539
BATT	-111.843	42.215
BEAR	-111.421	41.934
BECH	-111.046	44.149
BF10	-112.788	41.716
BIGB	-113.023	43.396
BIGT	-110.569	44.405
BIGU	-111.192	44.898
BIRC	-112.757	43.960
BLUF	-110.375	44.662
BOGS	-110.381	44.696
BORD	-111.047	42.195
BOXM	-112.015	41.636
BOZE	-111.046	45.663
BUSH	-112.338	43.540
BUTT	-112.518	45.968
C157	-110.702	44.970
CALM	-112.233	41.785
CEDA	-112.689	41.640
CIRC	-112.633	43.830
CNDR	-113.345	43.619
COBB	-112.920	43.508

Table S-2. Continued.

Station	Longitude	Latitude
CORA	-111.543	41.237
CRAT	-113.148	43.592
CURV	-112.003	41.757
CV17	-110.298	44.550
CV23	-110.386	44.568
CV24	-110.276	44.517
D092	-111.356	44.656
DICK	-113.927	44.179
DIKE	-112.094	41.342
DILL	-112.615	45.232
DONK	-113.560	44.266
DRYC	-111.788	41.735
E11A	-110.455	44.641
E138	-111.958	44.598
ECWA	-110.383	44.508
ELKA	-110.455	44.641
F011	-111.326	44.473
F014	-111.783	45.693
F145	-111.783	45.693
F575	-111.697	45.498
FLAG	-110.667	44.100
FRAN	-110.354	44.413
G103	-111.250	45.269
G498	-111.742	45.794
GILM	-113.251	44.504
GOLD	-112.601	41.668
GPSB	-104.867	41.134
GRAF	-113.056	43.665
GRAN	-110.993	43.769
GRAS	-110.820	44.132
GREY	-108.028	44.493
GRNT	-113.970	43.994
GRTA	-110.993	43.769
GT01	-110.613	43.761
GT12	-110.668	43.754
GT24	-110.726	43.750
GT35	-110.755	43.767
GT39	-110.785	43.764
GWM2	-110.245	44.903
H146	-111.679	45.232
HAET	-112.787	41.776
HANS	-112.667	41.918

Table S-2. Continued.

Station	Longitude	Latitude
HARD	-113.032	41.835
HARL	-110.889	44.640
HEBG	-111.335	44.864
HELE	-111.992	46.586
HOLL	-110.495	44.723
HOLM	-110.856	44.819
HORS	-111.197	44.751
HOTS	-110.257	44.744
HOWE	-112.544	41.794
HULL	-110.992	44.660
HUNT	-108.851	45.038
I107	-112.068	43.481
I762	-112.222	42.696
ID76	-112.222	42.696
IDTD	-116.230	43.634
INDI	-113.307	41.911
IUTW	-111.047	42.002
J011	-111.312	44.387
J041	-110.636	43.805
J161	-111.215	45.096
JOHN	-110.950	43.890
K092	-111.514	44.598
KAYG	-110.464	44.663
KELT	-113.252	41.696
L011	-111.305	44.317
LARD	-111.975	41.383
LATH	-111.145	44.448
LEHA	-110.387	44.600
LEWI	-110.635	44.268
LION	-111.348	44.724
M146	-111.656	45.112
M157	-110.733	44.888
MALL	-110.785	44.467
MASN	-110.330	42.714
MEER	-110.819	44.454
MISS	-114.090	46.924
MONT	-111.518	41.422
MORA	-110.721	43.866
N056	-112.698	43.326
N144	-111.479	44.830
NEZP	-110.820	44.573
O033	-111.144	44.658

Table S-2. Continued.

Station	Longitude	Latitude
ODGD	-111.882	41.200
P012	-110.002	44.490
PELI	-110.193	44.648
PIHA	-112.591	42.913
PITS	-110.473	44.520
POCR	-112.423	42.855
POON	-111.445	44.563
PORP	-113.955	43.931
PROM	-112.420	41.298
R011	-110.390	44.890
R015	-113.927	44.179
R046	-110.851	43.498
R161	-111.075	44.964
R415	-115.780	43.181
REST	-111.592	44.902
RGBY	-111.920	43.657
ROCK	-112.508	41.490
ROOF	-111.463	44.942
ROSE	-113.619	41.626
S058	-112.956	43.456
S138	-111.236	44.801
SALM	-113.869	45.166
SALN	-112.491	41.243
SARG	-110.643	43.938
SHOG	-114.417	42.936
SHOS	-110.644	44.434
SIDE	-112.148	41.795
SKYU	-111.649	44.713
SODA	-111.584	42.654
SOUT	-110.355	44.330
SPLT	-112.635	43.445
SPRU	-110.615	44.552
STAN	-114.944	44.226
STON	-110.325	44.594
TERN	-110.260	44.668
TERR	-112.230	43.839
TESA	-110.511	43.840
THAT	-112.342	41.721
THER	-110.833	44.516
TONI	-110.956	44.413
TREM	-112.184	41.711
TROU	-110.505	44.616

Table S-2. Continued.

Station	Longitude	Latitude
U11X	-111.806	43.834
U127	-111.780	41.767
U146	-111.651	44.989
U419	-115.890	42.466
U59A	-111.106	43.738
V297	-111.263	44.684
W367	-110.457	44.642
WARR	-112.239	41.255
WASH	-110.434	44.798
WELL	-111.909	41.651
WHEE	-113.105	41.746
WOOD	-114.030	43.433
X137	-111.756	44.592
Y053	-108.790	45.714
Y368	-110.063	44.979
Y425	-113.739	42.567
Y538	-108.790	45.714
YELL	-110.394	44.552
Z139	-111.718	45.597
Z145	-111.732	45.359
Z157	-110.699	44.738
Z161	-111.105	44.796
Z367	-110.489	44.679
Z425	-113.987	44.008

Table S-3. Permanant GPS stations in the Wasatch Network.

Station	Longitude	Latitude	Operating Agency
ALUT	-111.620	40.584	UU
DCUT	-111.527	40.414	UU
GOUT	-111.897	39.914	UU
MOUT	-111.666	41.046	UU
NAIU	-112.230	41.016	UU
RBUT	-111.809	40.781	UU
CAST	-110.677	39.191	PBO
CEDA	-112.860	40.681	PBO
COON	-112.121	40.653	PBO
EOUT	-111.929	41.253	PBO
FORE	-111.380	40.512	PBO
HEBE[a]	-111.373	40.514	PBO
HWUT	-111.565	41.607	PBO
LMUT	-111.928	40.261	PBO
LTUT	-112.247	41.592	PBO
MPUT	-111.634	40.016	PBO
SMEL	-112.845	39.426	PBO
SPIC	-112.127	39.306	PBO
P016	-112.361	40.078	PBO
P030	-110.513	41.750	PBO
P057	-112.623	41.757	PBO
P081	-113.871	39.067	PBO
P082	-113.505	39.269	PBO
P084	-113.054	40.494	PBO
P086	-112.282	40.649	PBO
P088	-111.723	40.772	PBO
P089	-111.415	40.807	PBO
P100	-113.294	41.857	PBO
P101	-111.236	41.692	PBO

Table S-3. Continued.

Station	Longitude	Latitude	Operating Agency
P103	-113.042	39.345	PBO
P103	-113.042	39.345	PBO
P104	-112.717	39.186	PBO
P105	-112.504	39.388	PBO
P106	-112.262	39.459	PBO
P108	-111.945	39.589	PBO
P109	-111.651	39.597	PBO
P110	-111.571	39.715	PBO
P111	-113.012	41.817	PBO
P112	-111.450	39.817	PBO
P113	-113.278	40.671	PBO
P114	-112.528	40.634	PBO
P115	-112.428	40.474	PBO
P116	-112.014	40.434	PBO
P117	-111.751	40.435	PBO
P118	-111.350	40.635	PBO
P119	-111.258	40.732	PBO
P121	-112.698	41.803	PBO
P122	-112.332	41.635	PBO
P124	-111.957	41.558	PBO
P125	-111.899	41.589	PBO
P126	-111.781	41.583	PBO
P675	-112.719	42.212	PBO
P783	-111.415	40.808	PBO
P783	-111.415	40.808	PBO
MIDV	-111.907	40.621	NGS
MYT1[a]	-110.048	40.103	NGS
MYT5	-110.048	40.103	NGS
SLCU	-111.955	40.772	NGS
ZLC1	-111.952	40.786	NGS

[a]Station has been retired and is no longer operating.

Table S-4. Temporary stations from the Wasatch field campaigns.

Station	Longitude	Latitude
1010	-111.717	40.752
1012	-120.177	38.633
1710	-111.639	40.644
3207	-116.746	39.056
0006	-113.520	39.094
0007	-110.352	38.964
010B	-119.697	39.285
026A	-112.030	40.847
0H64	-111.949	40.162
120F	-112.852	41.220
1S2E	-111.717	40.752
2S3E	-111.651	40.647
36UA	-111.426	40.483
3S3E	-111.621	40.584
43JD	-119.658	39.848
67LA	-114.055	36.833
84DO	-113.565	36.979
88JD	-114.701	41.905
A121	-111.720	40.219
ABRA	-112.110	41.111
AERO	-112.513	39.387
AIRP	-114.044	36.098
ANTE	-112.216	40.962
B300	-119.244	38.988
B365	-113.636	37.126
B423	-115.110	41.099
BAIR	-112.064	41.539
BARR	-113.474	40.728
BEAR	-111.421	41.934
BENN	-112.235	41.042
BF10	-112.788	41.716
BLAC	-113.604	37.095
BLAC	-119.058	39.579
BLAN	-109.483	37.581
BLMB	-111.951	40.720
BLUE	-110.284	40.216
BOUN	-111.818	40.964
BRYC	-112.154	37.704
BRZ2	-112.157	37.699
C021	-109.369	38.134
C137	-112.498	37.030

Table S-4. Continued.

Station	Longitude	Latitude
C313	-115.220	37.529
CANE	-112.901	36.846
CAPS	-112.047	39.662
CARL	-111.888	40.728
CDAR	-111.945	39.625
CDCA	-113.094	37.700
CESS	-112.355	38.964
CHAL	-119.876	39.514
CHER	-111.835	40.515
CHIL	-119.203	39.358
CISC	-109.303	38.959
CLIF	-117.418	39.351
CNYA	-109.751	38.762
CORA	-111.543	41.237
CURV	-112.003	41.757
D104	-110.745	40.209
DALE	-111.751	40.755
DAVI	-117.884	38.760
DELO	-108.976	38.683
DEVI	-114.031	37.728
DRYL	-114.842	37.615
DUDE	-111.838	40.831
EAGL	-119.483	39.552
ELBE	-111.950	39.952
ENVB	-114.024	40.726
ERDA	-112.253	40.635
ERM2	-114.843	39.293
F182	-112.985	38.617
F381	-113.809	41.430
FERN	-112.104	39.762
FLAT	-119.203	39.944
FLOR	-112.027	40.588
FOOT	-111.746	39.744
FRPK	-111.852	41.082
G100	-112.148	39.601
G101	-112.151	39.602
G200	-112.242	39.140
G250	-111.738	38.904
G365	-113.701	37.165
GENE	-111.719	40.298
GOG2	-112.049	40.813
GOGA	-112.049	40.813

Table S-4. Continued.

Station	Longitude	Latitude
GPS1	-111.843	40.760
GRA2	-111.818	40.573
GRAI	-111.904	40.758
GROV	-112.033	40.525
GX46	-118.311	39.274
H100	-111.020	39.293
H226	-120.325	39.318
HATT	-112.427	38.840
HEAV	-111.539	40.170
HIGH	-111.804	40.653
HOLA	-111.788	40.627
HOLD	-112.291	39.178
HOPE	-109.023	40.863
HOWE	-112.544	41.794
INLE	-111.900	40.357
IRON	-113.231	37.744
J334	-114.040	40.731
JIMM	-113.623	37.000
JORD	-111.415	40.594
K112	-110.695	38.413
KEAR	-111.971	40.643
KENT	-112.056	40.628
KERR	-112.133	40.708
KIMB	-111.538	40.741
KNBA	-112.531	37.010
LAGE	-114.625	40.058
LAK1	-112.211	38.341
LAKE	-114.652	38.541
LAKE	-112.254	40.702
LGUA	-111.865	41.790
LGUC	-111.854	41.785
LOMA	-108.821	39.309
M043	-111.707	39.206
MAGU	-119.790	39.367
MEEK	-107.893	40.042
MILL	-110.816	39.544
MONA	-111.853	39.807
MONR	-112.129	38.629
MONT	-111.518	41.422
MONY	-109.113	37.389
MORG	-111.744	41.041
MOST	-109.047	39.193

Table S-4. Continued.

Station	Longitude	Latitude
MRPH	-111.930	40.435
MUHA	-112.023	40.727
N373	-109.861	37.183
NGS2	-111.830	40.766
OGDA	-112.012	41.196
P115	-110.168	37.649
P208	-119.923	39.111
PIR1	-111.892	40.494
PIR8	-111.892	40.512
PIRC	-111.853	40.722
PLAT	-109.787	38.554
PLMM	-104.726	40.183
POLE	-111.538	40.028
PRIC	-110.754	39.610
QUI2	-111.790	39.940
R376	-113.055	37.780
RAT2	-118.703	39.995
REF2	-112.110	41.111
RICH	-112.086	38.778
RIVE	-111.910	40.531
ROOZ	-110.043	40.279
ROPE	-111.905	40.713
RUSS	-111.855	40.524
SAGE	-120.039	39.791
SALE	-110.306	39.033
SALI	-111.843	38.971
SANT	-111.826	39.978
SGUA	-113.593	37.088
SIDE	-112.148	41.795
SIMP	-112.917	40.182
SINK	-111.748	41.214
SLCF	-111.968	40.788
SORE	-113.961	39.051
SPRI	-111.697	40.159
STEE	-111.357	38.014
SUR1	-111.892	40.675
T23S	-111.317	38.778
THIS	-111.494	40.000
TIMP	-112.636	40.743
TREM	-112.184	41.711
U127	-111.780	41.767
U34A	-110.228	38.962

Table S-4. Continued.

Station	Longitude	Latitude
U42E	-111.995	40.628
U43A	-109.347	37.936
U69A	-110.385	40.194
U836	-120.325	39.318
UNI2	-111.886	40.582
UNIN	-111.886	40.582
UNIO	-111.886	40.582
UTES	-111.847	40.768
V175	-112.409	40.337
V209	-119.544	39.083
VABM	-111.810	40.730
VELA	-109.512	40.444
VER2	-109.570	40.337
VIEW	-111.853	40.463
VIST	-119.698	39.533
WARR	-112.239	41.255
WASZ	-113.432	36.502
WELL	-111.909	41.651
WEST	-112.063	40.565
WHEE	-113.105	41.746
WILL	-112.007	40.435
X364	-113.556	37.114
Y078	-113.208	39.629
Y419	-109.049	40.271
YARD	-111.941	40.731
ZLCA	-111.953	40.785
ZLCB	-111.951	40.785